Chemical Science

ROYAL SOCIETY OF CHEMISTRY

EDGE ARTICLE

View Article Online
View Journal | View Issue

Cite this: *Chem. Sci.*, 2025, **16**, 21010

All publication charges for this article have been paid for by the Royal Society of Chemistry

Received 23rd June 2025
Accepted 3rd October 2025

DOI: 10.1039/d5sc04596g

rsc.li/chemical-science

Isomeric decker metallo-supramolecules with tunable luminescence and chiroptical properties

Ningxu Han,[a] Jianjun Ma,[b] Hao Yu,[a] Junjuan Shi,[a] Manman Dai,[a] Ziteng Guo,[a] Zinuo Gao,[a] Houyu Zhang *[a] and Ming Wang *[a]

The regulation of interchromophoric interactions in multichromophoric systems is crucial for developing high-performance photofunctional materials. In this study, we present a novel self-assembly strategy to construct isomeric decker complexes, denoted as **S1** and **S2**, which integrate disparate chromophores, achiral BODIPY and chiral binaphthyl moieties. This isomerization results in distinct chromophore packing modes. In the case of **S1**, the BODIPY and binaphthyl moieties are arranged in a relatively loose manner (~6.0 Å), enabling efficient FRET and preserving the strong locally excited (LE) emission (Φ_F = 91.3%) characteristic of the BODIPY unit. In contrast, for **S2**, the denser packing between the BODIPY and binaphthyl moieties (~4.8 Å) leads to through-space charge transfer (TSCT) and weak charge transfer (CT) emissions (Φ_F = 8.6%). Notably, only complex **(R)/(S)-S1** shows mirror-image circular dichroism (CD) signals based on chirality transfer and circularly polarized luminescence (CPL), as supported by TD-DFT calculations, which reveal that the binaphthyl moiety alters the angle between the electric transition dipole moment (μ) and the magnetic transition dipole moment (*m*).

Introduction

The interplay between chromophores is pivotal in nature, as exemplified by the excitation energy transfer (EET) observed among chromophores such as chlorophylls, carotenoids, and phycobilins in photosynthetic organisms.[1] These chromophores can be organized into particular arrangements by the surrounding protein scaffolds, resulting in modulated excitonic interactions that optimize the light-harvesting properties and EET efficiency, crucial for transforming solar energy into chemical energy.[2] Inspired by nature, researchers realize that the fine-tuning of chromophore arrangements is crucial for efficient interchromophoric interactions, thereby improving material performance in relation to light-harvesting,[3–7] emission,[8–12] and chiral fields.[13–16] In this context, artificial synthetic skeletons capable of manipulating the chromophore arrangements have garnered increasing attention. In multichromophoric systems, many through-space interactions, such as EET,[17–20] through-space charge transfer (TSCT),[21–24] and chirality transfer,[25–27] are mainly governed by specific spatial orientations and distance between chromophores. For instance, efficient energy transfer between donor and acceptor chromophores typically requires a distance of less than 10 nm due to dipole–dipole coupling.[28,29] When an electron-rich donor and an electron-deficient acceptor are positioned in a close face-to-face manner, with a spatial distance of ~4 Å, a CT interaction can occur and lead to a new excited state with a narrowed energy gap. Notably, when a chiral chromophore is strategically oriented relative to an achiral counterpart, it can establish a chiral microenvironment around the achiral molecules, facilitating chirality transfer and inducing their chiroptical properties. Currently, significant efforts are being devoted to exploring suitable synthetic skeletons capable of precisely regulating chromophore arrangements, thereby advancing the understanding of structure–performance relationships.

Isomerism of photofunctional molecules represents a powerful strategy for precisely controlling the spatial arrangement of functional groups, thereby optimizing material performance. For organic molecules, common strategies to achieve isomerism (Fig. 1) involve either modifying identical chromophore or substituent pairs at distinct positions within the same molecular skeleton (regioisomerism),[30–34] or utilizing photoswitches as molecular skeletons to facilitate *trans*-to-*cis* isomerization (stereoisomerism).[35–40] For example, Tang *et al.* regulated the packing mode and solid-state fluorescence of isomeric molecules by tuning the substituted positions of chromophores.[41] Furthermore, the isomerism strategy can be employed to tailor organic ligands, enabling the facile synthesis of isomeric metallo-supramolecules[42–46] or metal–organic frameworks.[47–50] For example, Nitschke *et al.* prepared isomeric coordination cages by employing isomeric anthracene-based ligands and studied their stimuli-driven guest uptake and release.[51] These innovative strategies inspire the modulation of

[a]*State Key Laboratory of Supramolecular Structure and Materials, College of Chemistry, Jilin University, Changchun, Jilin 130012, China. E-mail: mingwang358@jlu.edu.cn; houyuzhang@jlu.edu.cn*

[b]*Engineering Research Center of Xinjiang and Central Asian Medicine Resources, Ministry of Education, Xinjiang Medical University, Urumqi, Xinjiang 830011, China*

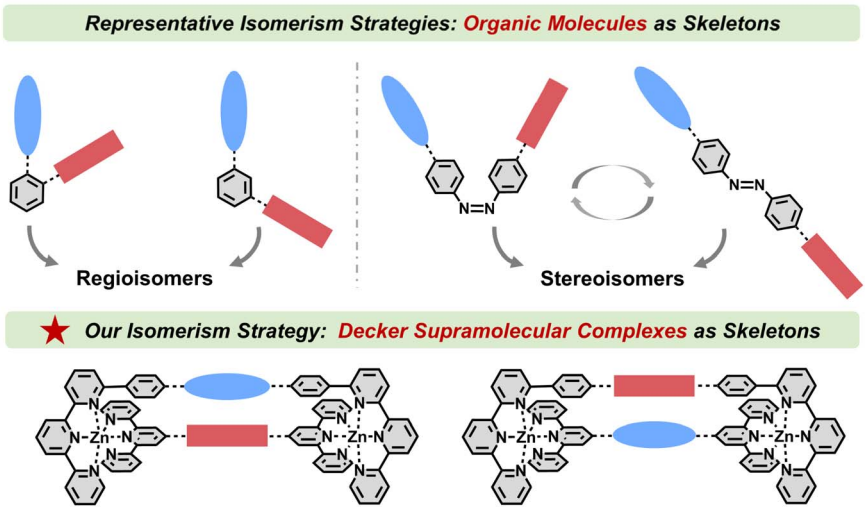

Fig. 1 Examples of previous isomerism strategies and our proposed isomerism strategy based on decker supramolecular skeletons in this work.

chromophore arrangements and properties through the application of isomerism. However, examples demonstrating modulation of through-space chromophore interactions *via* isomerism-driven subtle adjustments of chromophore arrangements remain limited. This could be attributed to the following two reasons: (1) the challenges in designing molecular skeletons capable of simultaneously achieving isomerism and effective through-space interactions and (2) rigid interchromophoric interactions that are resistant to modulation through subtle alterations in spatial arrangements.

Herein, we propose a novel design strategy to realize the regioisomerism of heterochromophore decker complexes **S1** and **S2** with well-defined geometry (Fig. 2). Two types of functional chromophores, boron-dipyrromethene (BODIPY) and binaphthyl moieties, are incorporated into each of the complexes. By employing dissymmetrical modified 2,2′:6′,2″-terpyridine (tpy) units, two chromophores can be precisely placed in close spatial proximity, which provides a suitable model for the comparative study of interchromophoric interactions in isomeric systems. It is impressive that these two isomeric decker complexes show completely different photophysical processes, confirmed by photophysical characterization and DFT and TD-DFT calculations. Complex **S1** exhibits outstanding LE emission, while complex **S2** shows quenched CT emission. Additionally, compared with significant chirality transfer from **LB** to **LA** in **S1**, no similar phenomenon is observed in **S2**. These findings demonstrate that our decker supramolecular skeleton enables isomeric modification and adjustable interactions between chromophores, offering significant insights for the development of high-performance emissive and chiral materials.

Results and discussion

Synthesis and characterization of heterochromophore decker complexes

We designed and synthesized four tpy ligands, in which **LA** and **LD** contain a BODIPY moiety and enantiopure ligands **LB** (ref.

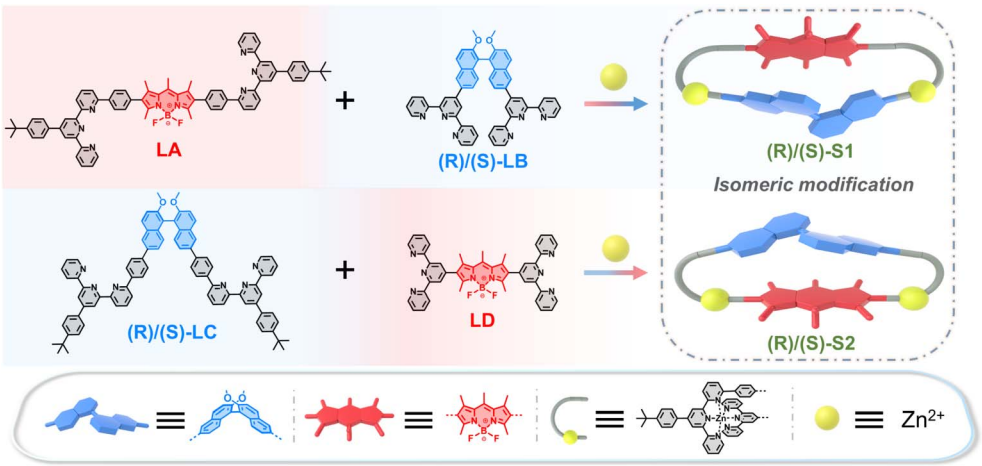

Fig. 2 Design and self-assembly of ligands and isomeric decker complexes.

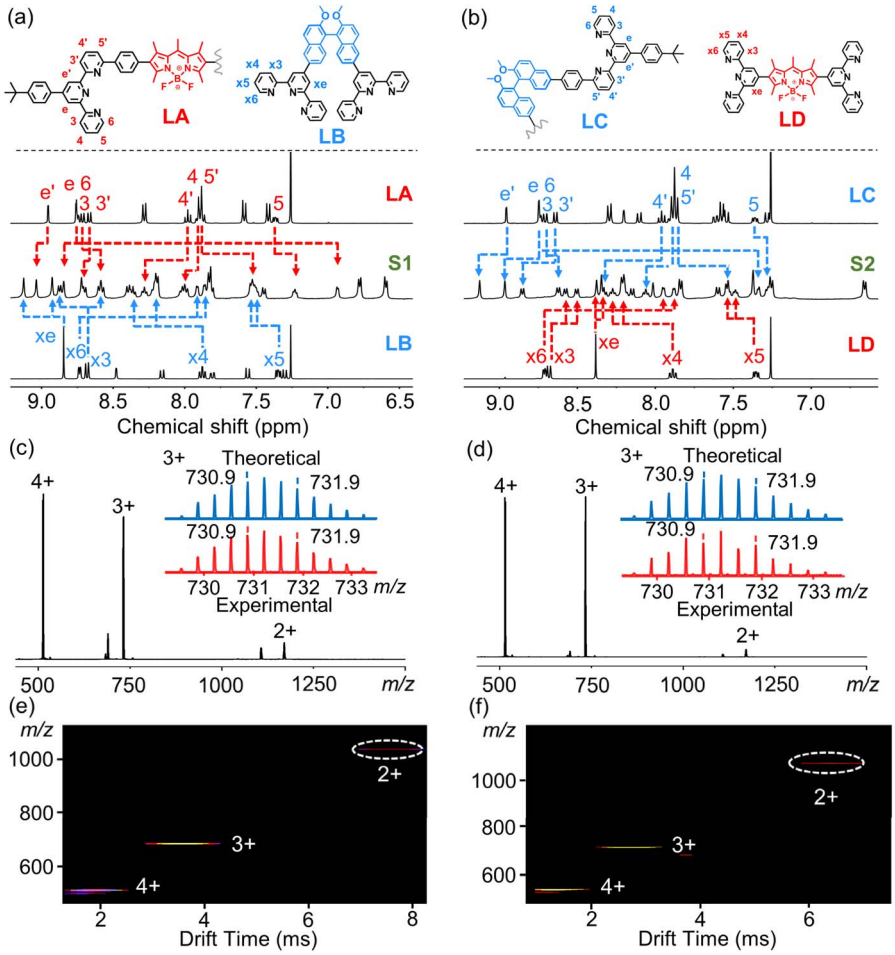

Fig. 3 ^{1}H NMR spectra (400 MHz, 298 K) of (a) ligands **LA** and **LB** in $CDCl_3$ and complex **S1** in CD_3CN and (b) ligands **LC** and **LD** in $CDCl_3$ and complex **S2** in CD_3CN. ESI-MS spectra of complexes (c) **S1** and (d) **S2**. TWIM-MS spectra of complexes (e) **S1** and (f) **S2**.

52) and **LC** contain a chiral binaphthyl moiety, all in decent yields. The synthetic procedures and full characterization by ^{1}H and ^{13}C nuclear magnetic resonance (NMR) spectroscopy, two-dimensional correlation spectroscopy (2D-COSY), and matrix-assisted laser desorption/ionization time-of-flight (MALDI-TOF) mass spectrometry of all ligands are shown in the SI (Fig. S1 and S4–S18). Isomeric complexes **S1** and **S2** were assembled by mixing the ditopic ligands **LA** and **LB** for **S1**, and ligands **LC** and **LD** for **S2**, respectively, with $Zn(NO_3)_2 \cdot 6H_2O$ in exact stoichiometric ratios of 1 : 1 : 2 in $CHCl_3$/MeOH at 50 °C for 10 h. Following the excess addition of NH_4PF_6, red complexes were obtained without further purification.

NMR spectroscopy was employed to confirm the generation of the complexes. As shown in Fig. 3a and b, ^{1}H-NMR spectra of these two complexes exhibited sharp and well-resolved proton signals, indicating the probable construction of discrete assemblies. NMR resonances of complexes were further assigned by 2D-COSY and nuclear Overhauser effect spectroscopy (NOESY) (Fig. S19–S30). In contrast to the rigid, linearly configured BODIPY-based ligands, **LB** and **LC** showed flexible geometries, resulting from axially chiral binaphthyl cores. Upon complexation, the conformations of both **LB** and **LC** were strongly rigidified, resulting in a distinct chemical environment of the tpy protons within each ligand. Through accurate integration analysis, the stoichiometries of different ligands in the complexes were proved to be 1 : 1, as expected for isomeric complexes. Diffusion-ordered NMR spectroscopy (DOSY) showed that all the protons of each complex had the same band (Fig. S33 and S34), consistent with discrete assemblies with a single component. Electrospray ionization mass spectrometry (ESI-MS) showed a set of prominent peaks arising from consecutive charge states (2+ to 4+) due to the loss of anions (PF_6^-), consistent with the expected heteroleptic complexes (Fig. 3c and d). In addition, the experimental isotope patterns of each charge state matched well with their simulated counterparts (Fig. S2 and S3). Traveling wave ion mobility-mass spectrometry (TWIM-MS) displayed the narrow drift time distributions of each charge state for the complexes (Fig. 3e and f), indicative of the formation of a single product.

A single crystal of complex **(R)-S1** was obtained by slow vapor diffusion of ethyl acetate into the MeCN solution of complex **(R)-S1** over a period of 4 weeks. The single-crystal structure of complex **S1** validated the precision of our heteroleptic self-assembly strategy, where ligand **LA** with six-position-modified tpy units selectively bound ligand **LB** based on shape complementary assembly (Fig. 4a).[53,54] To accommodate the rigid

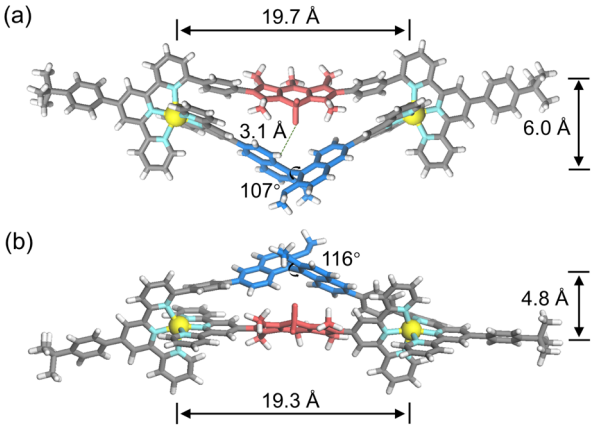

Fig. 4 (a) X-ray crystal structure of complex (R)-S1. (b) DFT model of (S)-S2. All solvent molecules and counterions are omitted for clarity.

ligand **LA** with a fixed arm length, the axially chiral binaphthyl core with adaptable configuration adopted a specific twist, where the dihedral angle of two different naphthyl planes was ~107°. The methoxy groups adopted the orientation outward the sterically crowded triangular cavity of complex **S1**. The C–H···F hydrogen bond interactions (~3.1 Å) were observed between binaphthyl protons and fluorine atoms in BODIPY units. A DFT-optimized model of **S2** is shown in Fig. 4b, and it exhibited a more congested triangular cavity, as evidenced by the reduced Zn···Zn distance (~19.3 Å) and interchromophoric distance (~4.8 Å) compared to those in **S1** (~19.7 and 6.0 Å, respectively).

Photophysical properties

The photophysical properties of all ligands and complexes in solution were investigated using UV–vis absorption and fluorescence spectroscopy. The absorption spectra of ligands **LB** and **LC** (10 μM in $CHCl_3$) exhibited broad bands between 250 and 375 nm (Fig. S36a). In contrast, ligands **LA** and **LD** displayed additional absorption bands in the range of 450–580 nm (Fig. S35a), centered at 529 nm and 521 nm, respectively, which mainly originated from the electronic transitions of BODIPY moieties. To further understand the photophysical properties of ligands, we performed quantum-chemical calculations using DFT and TD-DFT methods. In ligands **LA** and **LD**, the highest occupied molecular orbitals (HOMOs) and the lowest unoccupied molecular orbitals (LUMOs) are mainly located on the BODIPY moieties (Fig. S50), indicative of negligible CT character. The lowest-energy absorption bands of ligands **LA** and **LD** are mainly ascribed to the HOMO → LUMO transitions, with high oscillator strengths (*f*) of 1.26 and 1.18, respectively. For ligands **LB** and **LC**, the HOMOs are mainly located on the binaphthyl units, whereas the LUMOs are concentrated on the tpy moieties (Fig. S51). The lowest-energy absorption bands of ligands **LB** and **LC** arise mainly from HOMO → LUMO and HOMO → LUMO+2 transitions (Fig. S51), with corresponding oscillator strengths of 0.65 and 0.60, respectively.

The photoluminescence (PL) spectra of all the ligands (Fig. S35b and S36b) exhibited intense emission bands with maximum emission wavelengths at 573 nm, 409 nm, 396 nm, and 546 nm for **LA**, **LB**, **LC**, and **LD**, respectively. Their photoluminescence quantum yields (Φ_F) and lifetimes in $CHCl_3$ are determined as follows: 99.7% and 4.37 ns for **LA**, 51.6% and 4.37 ns for **LB**, 67.0% and 1.53 ns for **LC**, and 99.8% and 4.42 ns for **LD**, respectively (Fig. S46, S47 and Table S1). For binaphthyl-based ligands **LB** and **LC**, pronounced solvatochromism behavior was observed (Fig. S38 and S39), as a result of the CT transition from binaphthyl to tpy moieties. On the other hand, such a phenomenon was absent for BODIPY-based ligands **LA** and **LD** (Fig. S37 and S40), indicative of their weak CT character. Despite the different coordination units (six-position-modified or unmodified tpy) attached to the BODIPY moiety, both

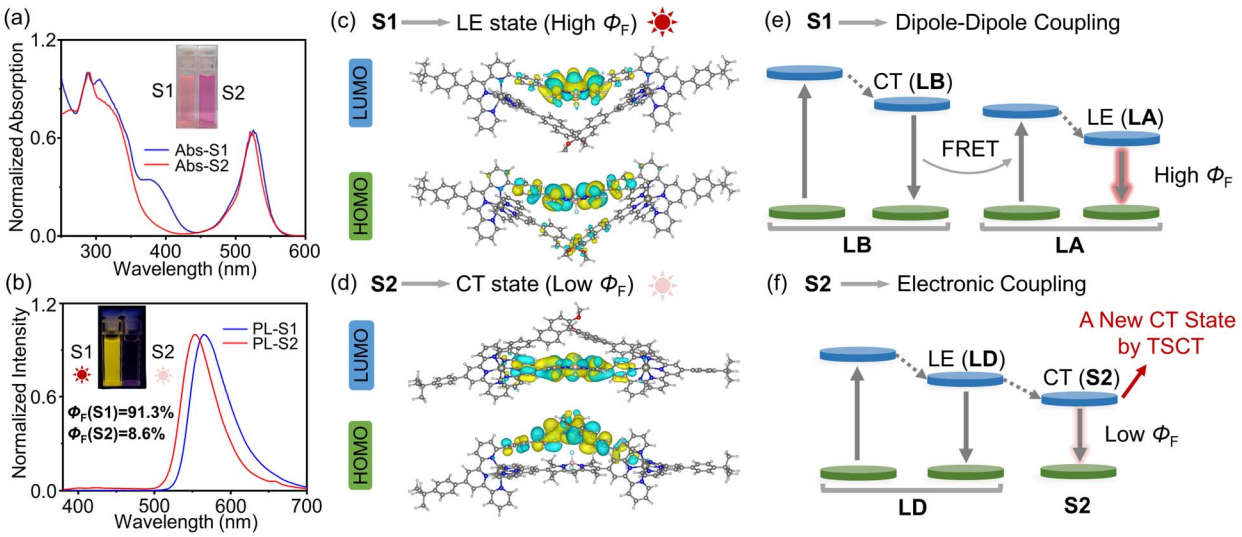

Fig. 5 (a) Absorption and (b) fluorescent emission spectra (λ_{ex} = 330 nm) of complexes **S1** and **S2** at the concentration of 10 μM in CH_3CN. Insets: photographs of complexes **S1** and **S2** in CH_3CN under visible light (a) and under 365 nm UV light (b). Molecular orbitals of complexes (c) (R)-S1 and (d) (S)-S2 calculated using TD-DFT. Comparison of proposed photophysical processes in complexes (e) **S1** and (f) **S2**.

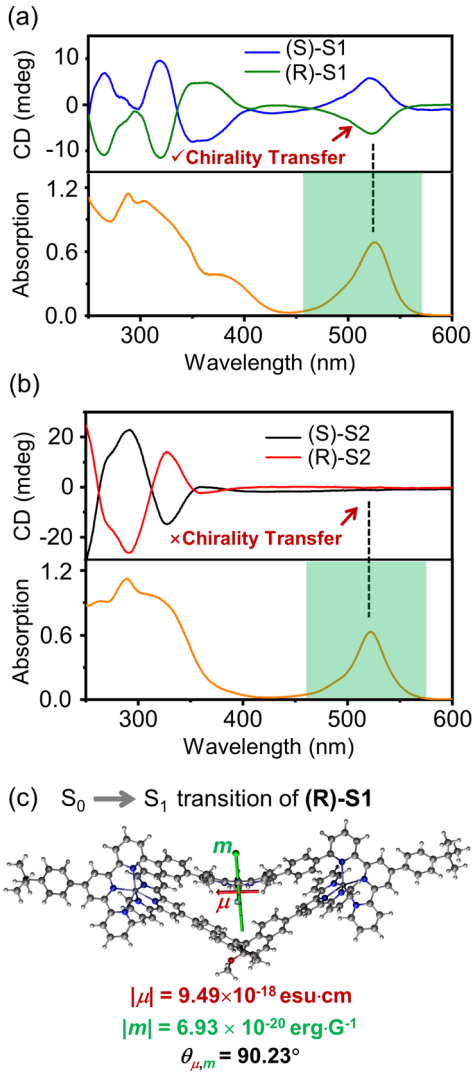

Fig. 6 CD and absorption spectra ($c = 10$ μM) of complexes (a) (R)/(S)-S1 and (b) (R)/(S)-S2 in CH_3CN. (c) $S_0 \rightarrow S_1$ transition electric and magnetic dipole moments of (R)-S1. The transition magnetic dipole moment vector is shown in green and the transition electric dipole moment vector is shown in red.

ligands **LA** and **LD** show exceptional photoluminescence quantum yields in $CHCl_3$, indicative of the negligible perturbation of these substituents to the intrinsic emissive properties of the BODIPY moiety.

For complexes, **S1** and **S2** exhibited broad absorption bands between 250 and 440 nm and a strong absorption peak at 525 nm for **S1** and 522 nm for **S2** in CH_3CN, respectively (Fig. 5a). Despite containing two different ligands, both complexes exhibited single emission bands in CH_3CN (10 μM; $\lambda_{ex} = 330$ nm), with maximum emission wavelengths at 564 nm for **S1** and 554 nm for **S2** (Fig. 5b), respectively, attributed to the strong interplay between different ligands. Similar to highly emissive ligand **LA**, complex **S1** also showed excellent fluorescent properties in CH_3CN ($\Phi_F = 91.3\%$). However, complex **S2** exhibited dramatically quenched emission with a Φ_F of 8.6% in CH_3CN, notably lower than the high photoluminescence quantum yield of ligand **LD**. The pronounced disparity between the isomeric complexes **S1** and **S2** is tentatively attributed to the different through-space chromophore interactions.

To enable a comparative study between ligands and complexes, we investigated the optical properties of the ligands and complexes (NO_3^- as counterions) in the mixed solvent of $CHCl_3$/MeOH (v : v = 1 : 1), due to the good solubility of all the ligands and complexes (Fig. S41–S43). Both ligand **LA** and complex **S1** exhibited comparable absorption peaks between 470 and 600 nm and emission peaks, suggesting the nearly preserved electronic transition of ligand **LA** upon complexation. The perfect spectral overlap between **LB** emission and **LA** absorption bands (Fig. S43) facilitates efficient Förster resonance energy transfer (FRET), as evidenced by the dominant emission peak at 565 nm upon 330 nm excitation. In contrast, complex **S2** exhibited a broadened and red-shifted absorption band compared to ligand **LD**, accompanied by a corresponding red-shifted emission maximum at 557 nm. This spectral behavior was recapitulated in CH_3CN (Fig. S44 and S45), collectively supporting the hypothesis that through-space interactions within **S2** generate a new lowest-lying electronic state.

To elucidate the different photophysical behaviors of isomeric **S1** and **S2**, we performed quantum-chemical calculations using DFT and TD-DFT methods. In complex **S1**, the HOMOs and LUMOs are mainly located on the BODIPY moieties within ligand **LA** (Fig. 5c), suggesting negligible CT interactions between chromophores. The lowest-energy absorption band of complex **S1** is mainly attributed to the HOMO → LUMO transitions with a high oscillator strength of 0.93 (Fig. S52). Consequently, the highly emissive character of complex **S1** can be attributed to the LE state within ligand **LA**, with the binaphthyl moiety exerting minimal effect on **LA**'s electronic state. Conversely, the HOMOs and LUMOs of complex **S2** are mainly concentrated on binaphthyl and BODIPY moieties (Fig. 5d), respectively, indicating that the TSCT from the binaphthyl donor to the BODIPY acceptor plays a significant role in the photophysical processes. Notably, the HOMO → LUMO transitions of **S2** exhibit extremely low oscillator strengths (f <0.01), resulting in a negligible CT band in the absorption spectrum. The HOMO-2 → LUMO transitions with a high oscillator strength of 1.17 could account for the intense absorption peak at 522 nm (Fig. S53). However, this newly emerged lowest-lying electronic state, associated with the CT state, could have a significant impact on the emission process and explain the substantial reduction in PL quantum yields of complex **S2** relative to ligand **LD**.

The very different through-space interactions within isomeric complexes may originate from the varying chromophore arrangements and their attached skeleton molecules. The chromophore pair in complex **S2** exhibits a denser arrangement. As a result, the electronic coupling between binaphthyl and BODIPY moieties in complex **S2** is promoted and leads to a new CT state (Fig. 5f). On the other hand, the electron-deficient tpy moieties, directly attached to the BODIPY acceptor in ligand **LD**, could reduce the electron density on BODIPY, thereby facilitating TSCT in complex **S2**. Whereas in isomeric complex **S1**, the tpy moieties were attached to electron-

rich binaphthyl moieties, favoring dominant through-bond CT from binaphthyl to tpy moieties over TSCT. In addition, ligand **LB**, operating as a singular molecular entity, can behave as an energy donor in the FRET process of complex **S1** (Fig. 5e).

Chiroptical properties

The chiroptical properties of complexes **S1** and **S2** were further investigated by CD spectroscopy to explore the interactions between chiral ligands (**LB** or **LC**) and achiral ligands (**LA** or **LD**). The mirror-imaged CD signals were observed for **(R)/(S)-S1** and **(R)/(S)-S2**, corresponding to two pairs of enantiomers (Fig. 6a and b). Specifically, complex **(R)/(S)-S1** showed a CD signal between 460 and 550 nm, originating from the achiral ligand **LA** with the BODIPY chromophore, demonstrating the successful chirality transfer from the binaphthyl moiety to the BODIPY chromophore. This is in stark contrast to the silent CD signals of **(R)/(S)-S2** in this spectral range.

The chirality transfer observed in complex **(R)/(S)-S1** inspires us to explore the interaction mechanism by TD-DFT calculations. According to the theory, the dissymmetry factor for CD (g_{abs}) is determined by the transition electric dipole moment (μ), magnetic dipole moment (m), and the angle (θ) *via* the simplified equation $g_{abs} = 4\,(|m|/|\mu|)\cos\theta$.[55,56] According to the calculations of complex **S1**, the absorption band in this range could be assigned to $S_0 \rightarrow S_1$ transition associated with HOMO → LUMO transition. The HOMOs and LUMOs are mainly located on the BODIPY moieties within ligand **LA**, indicating minimal involvement of the binaphthyl moiety in this absorption feature. The μ and m as well as the angle between μ and m of **(R)-S1** for $S_0 \rightarrow S_1$ transitions were determined using calculations (Fig. 6c). It was found that the angle ($\theta = 90.23°$) has changed, deviating from 90°, leading to a negative $\cos\theta$ value (~ -0.004). This theoretical finding correlates well with the experimentally observed negative CD signal for **(R)-S1**.

To further validate the difference in chirality transfer behaviors of isomeric **S1** and **S2**, the CPL spectra of enantiomers **(R)/(S)-S1** and **(R)/(S)-S2** were measured in CH_3CN. As anticipated, **(R)/(S)-S1** exhibited mirror-image CPL signals, consistent with the chirality transfer properties observed from CD spectra, whereas **(R)/(S)-S2** showed no detectable CPL activity (Fig. 7a). According to the TD-DFT computational results, the HOMOs and LUMOs in the excited state are similar to those in the ground state (Fig. 7d), primarily localized on the BODIPY moiety, which effectively explains the nature of LE emission of

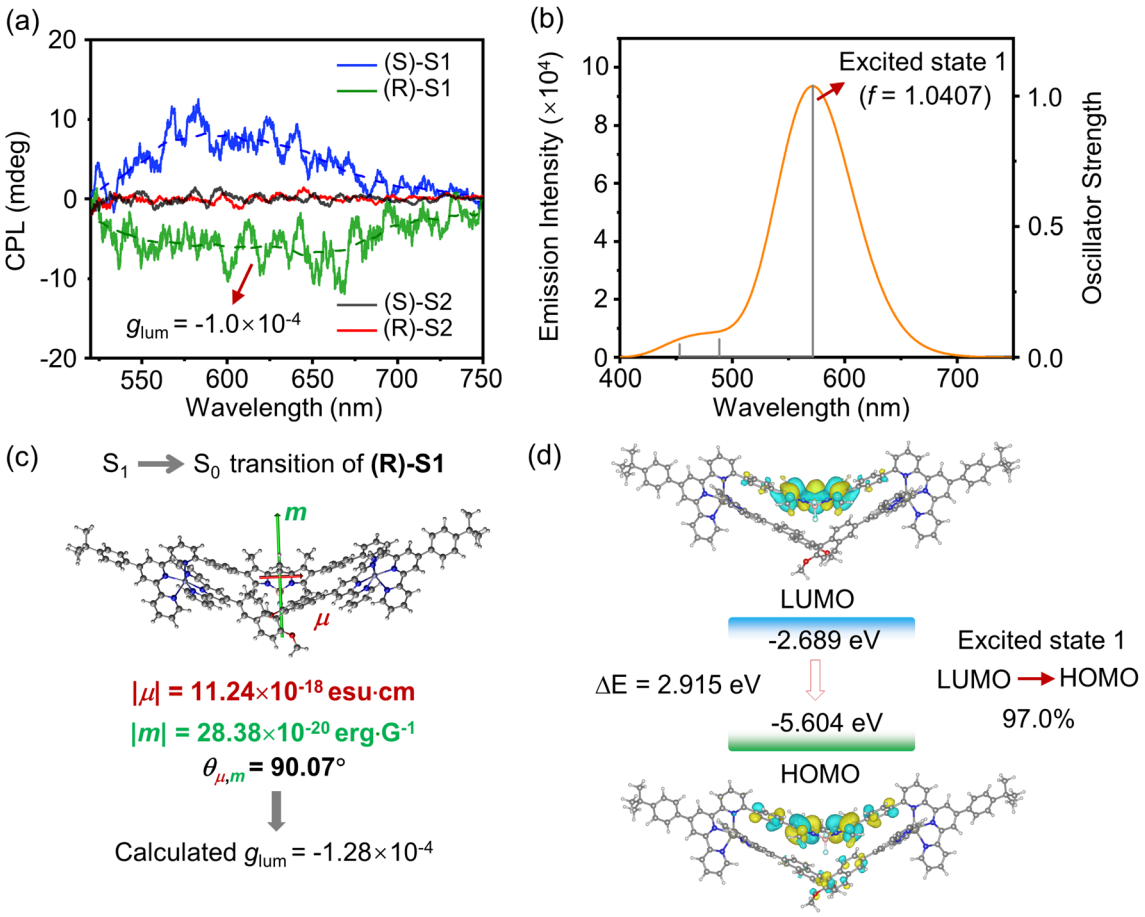

Fig. 7 (a) CPL spectra (c = 50 μM; λ_{ex} = 420 nm) of complexes **(R)/(S)-S1** and **(R)/(S)-S2** in CH_3CN. (b) TD-DFT calculated emission spectra of **(R)-S1** in CH_3CN. (c) $S_1 \rightarrow S_0$ transition electric and magnetic dipole moments of **(R)-S1**. The transition magnetic dipole moment vector is shown in green and the transition electric dipole moment vector is shown in red. (d) Molecular orbitals of complex **(R)-S1** in the excited states calculated using TD-DFT.

complex **S1**. Furthermore, the first excited state ($S_1 \rightarrow S_0$) is predominantly contributed by the LUMO → HOMO transition (97%) and exhibits the highest oscillator strength ($f = 1.0407$) (Fig. 7b), significantly higher than that of the second excited state ($S_2 \rightarrow S_0$). This further confirms that the main fluorescence and circularly polarized luminescence observed experimentally originate from the first excited state ($S_1 \rightarrow S_0$). Based on these findings, we further calculated m, μ, and θ for the first excited state. Using these values, a calculated g_{lum} value of -1.28×10^{-4} for **(R)-S1** was obtained (Fig. 7c), which is in agreement with the experimental result (-1.0×10^{-4}).

This chirality transfer property likely arises from the specific spatial arrangements between the binaphthyl and BODIPY moieties, encompassing factors such as spatial distance and relative orientation.[57–59] Unlike fluorescent groups with inherent chiral conformations, such as tetraphenylethylene[60–62] and perylene diimide,[63–65] whose chirality transfer mechanisms rely on the control of their chiral conformations, the crystal structure of **(R)-S1** reveals that the BODIPY moiety in ligand **LA** does not adopt a chiral conformation. This chirality transfer is likely attributed to the chiral microenvironment created by the binaphthyl moiety, which results in an altered angle between μ and m. Despite the closer proximity of the identical chromophore pair in **S2**, the absence of chirality transfer underscores the critical role of specific spatial orientation over mere proximity.

Conclusions

In summary, we propose a novel design strategy for engineering regioisomeric decker metallo-supramolecules with modulated interchromophoric interactions. The identical functional chromophore pair, binaphthyl and BODIPY moieties, is systematically introduced into the regioisomeric decker complexes **(R)/(S)-S1** and **(R)/(S)-S2**. The dense spatial arrangements of chromophores enable efficient interchromophoric interactions, specifically FRET in **S1** and TSCT in **S2**, as evidenced by integrated photophysical characterization and DFT and TD-DFT calculations. We attribute the different interactions to both the distinct chromophore arrangements and the conjugated skeleton molecules. **S2** exhibits a denser chromophore arrangement than **S1**, promoting the electronic coupling. Whereas the skeleton molecules (tpy and benzene) might also affect the electronic nature of the chromophores and their interactions. Furthermore, CD and CPL spectra confirmed the chirality transfer from the chiral binaphthyl to BODIPY moiety within complex **S1**, a phenomenon not observed in **S2** with similar chromophore arrangements. This successful chirality transfer in **S1** was unambiguously demonstrated by calculations. We attribute the chiral signal of the achiral BODIPY moiety to the chiral microenvironment created by the binaphthyl group, leading to changes in the angle between μ and m. This work exemplifies a unique case illustrating how isomeric modification can induce substantial variations in interchromophoric interactions, offering novel insights for the design of advanced photofunctional and chiroptical materials. Furthermore, the modular architecture of this system suggests promising potential for integrating diverse functional units, including luminogens, photoswitches, catalytic centers, radicals, therapeutic agents, or chiral groups, demonstrating its potential for broad applications across multiple disciplines.

Author contributions

M. W. conceived the study and designed the experiments. N. H., J. M., and J. S. conducted the experiments and analyzed the data. H. Y. collected the X-ray data and refined the structures. M. D., Z. G. and Z. G. performed the ESI-MS and TWIM-MS experiments. H. Z. conducted the DFT calculations. N. H., J. S., H. Z., and M. W. wrote the manuscript. All authors discussed the results and commented on the manuscript.

Conflicts of interest

There are no conflicts to declare.

Data availability

The data supporting this article have been included as part of the Supplementary Information (SI).

CCDC 2440691 contains the supplementary crystallographic data for this paper.[66]

Supplementary information: synthesis of the ligands and complexes, NMR spectra, MALDI-TOF spectra, ESI-MS data, single-crystal data, absorption spectra, fluorescent emission spectra, CD spectra, and CPL spectra. See DOI: **https://doi.org/10.1039/d5sc04596g**.

Acknowledgements

The authors are grateful for the support from the National Natural Science Foundation of China (22271116 for M.W. and 22491197 for J.S.), the Natural Science Foundation of Jilin Province (20230101027JC for M.W.), the fellowship of China Postdoctoral Science Foundation (2021M701383 for J.S.), and the staff at the BL17B1 beamline of the National Facility for Protein Science in Shanghai (NFPS), Shanghai Advanced Research Institute, CAS, for providing technical support for X-ray diffraction data collection and analysis. The project was supported by the Open Research Fund of State Key Laboratory of Polymer Physics and Chemistry, Changchun Institute of Applied Chemistry, Chinese Academy of Sciences.

Notes and references

1 G. D. Scholes, G. R. Fleming, A. Olaya-Castro and R. van Grondelle, Lessons from nature about solar light harvesting, *Nat. Chem.*, 2011, **3**, 763–774.

2 R. Croce and H. van Amerongen, Natural strategies for photosynthetic light harvesting, *Nat. Chem. Biol.*, 2014, **10**, 492–501.

3 M. Hecht and F. Würthner, Supramolecularly engineered J-aggregates based on perylene bisimide dyes, *Acc. Chem. Res.*, 2021, **54**, 642–653.
4 M. R. Wasielewski, Self-assembly strategies for integrating light harvesting and charge separation in artificial photosynthetic systems, *Acc. Chem. Res.*, 2009, **42**, 1910–1921.
5 Y. Hong, J. Kim, W. Kim, C. Kaufmann, H. Kim, F. Würthner and D. Kim, Efficient multiexciton state generation in charge-transfer-coupled perylene bisimide dimers *via* structural control, *J. Am. Chem. Soc.*, 2020, **142**, 7845–7857.
6 J. Gorman, S. R. E. Orsborne, A. Sridhar, R. Pandya, P. Budden, A. Ohmann, N. A. Panjwani, Y. Liu, J. L. Greenfield, S. Dowland, V. Gray, S. T. J. Ryan, S. De Ornellas, A. H. El-Sagheer, T. Brown, J. R. Nitschke, J. Behrends, U. F. Keyser, A. Rao, R. Collepardo-Guevara, E. Stulz, R. H. Friend and F. Auras, Deoxyribonucleic acid encoded and size-defined π-stacking of perylene diimides, *J. Am. Chem. Soc.*, 2022, **144**, 368–376.
7 D. Bialas, E. Kirchner, M. I. S. Röhr and F. Würthner, Perspectives in dye chemistry: a rational approach toward functional materials by understanding the aggregate state, *J. Am. Chem. Soc.*, 2021, **143**, 4500–4518.
8 C.-A. Shen, M. Stolte, J. H. Kim, A. Rausch and F. Würthner, Double J-coupling strategy for near infrared emitters, *J. Am. Chem. Soc.*, 2021, **143**, 11946–11950.
9 A. Garci, S. Abid, A. H. G. David, L. O. Jones, C. S. Azad, M. Ovalle, P. J. Brown, C. L. Stern, X. Zhao, L. Malaisrie, G. C. Schatz, R. M. Young, M. R. Wasielewski and J. F. Stoddart, Exciplex emission and Förster resonance energy transfer in polycyclic aromatic hydrocarbon-based bischromophoric cyclophanes and homo[2]catenanes, *J. Am. Chem. Soc.*, 2023, **145**, 18391–18401.
10 I. Regeni, R. Chowdhury, K. Terlinden, S. Horiuchi, J. J. Holstein, S. Feldmann and G. H. Clever, Engineering soluble diketopyrrolopyrrole chromophore stacks from a series of Pd(II)-based ravels, *Angew. Chem., Int. Ed.*, 2023, **62**, e202308288.
11 S.-Y. Yang, Y.-K. Wang, C.-C. Peng, Z.-G. Wu, S. Yuan, Y.-J. Yu, H. Li, T.-T. Wang, H.-C. Li, Y.-X. Zheng, Z.-Q. Jiang and L.-S. Liao, Circularly polarized thermally activated delayed fluorescence emitters in through-space charge transfer on asymmetric spiro skeletons, *J. Am. Chem. Soc.*, 2020, **142**, 17756–17765.
12 Y. Vonhausen, A. Lohr, M. Stalte and F. Würthner, Two-step anti-cooperative self-assembly process into defined π-stacked dye oligomers: insights into aggregation-induced enhanced emission, *Chem. Sci.*, 2021, **12**, 12302–12314.
13 L. Zhang, T. Wang, J. Jiang and M. Liu, Chiral porphyrin assemblies, *Aggregate*, 2023, **4**, e198.
14 Y. Xue, C. Zhang, T. Lv, L. Qiu and F. Wang, Amplification of dissymmetry for circularly polarized photodetection by cooperative supramolecular polymerization, *Angew. Chem., Int. Ed.*, 2023, **62**, e202300972.
15 T. Zhao, J. Yi, C. Liu, X. Liang, Y. Shen, L. Wei, X. Xie, W. Wu and C. Yang, "First come, first served" and threshold effects in a central-to-planar-to-helical hierarchical chiral induction, *Angew. Chem., Int. Ed.*, 2023, **62**, e202302232.
16 Y. Wang, W.-L. Zhao, Z. Gao, C. Qu, X. Li, Y. Jiang, L. Hu, X.-Q. Wang, M. Li, W. Wang, C.-F. Chen and H.-B. Yang, Switchable topologically chiral [2]catenane as multiple resonance thermally activated delayed fluorescence emitter for efficient circularly polarized electroluminescence, *Angew. Chem., Int. Ed.*, 2025, **64**, e202417458.
17 Y. Fan, S. Fan, L. Liu, S. Guo, J. He, X. Li, Z. Lian, W. Guo, X. Chen, Y. Wang and H. Jiang, Efficient manipulation of Förster resonance energy transfer through host–guest interaction enables tunable white-light emission and devices in heterotopic bisnanohoops, *Chem. Sci.*, 2023, **14**, 11121–11130.
18 N. Wang, Z. Wang, L. Chen, W. Chen, Y. Quan, Y. Cheng and H. Ju, Dual resonance energy transfer in triple-component polymer dots to enhance electrochemiluminescence for highly sensitive bioanalysis, *Chem. Sci.*, 2019, **10**, 6815–6820.
19 Y. Qin, L.-J. Chen, Y. Zhang, Y.-X. Hu, W.-L. Jiang, G.-Q. Yin, H. Tan, X. Li, L. Xu and H.-B. Yang, Photoswitchable Förster resonance energy transfer (FRET) within a heterometallic Ir–Pt macrocycle, *Chem. Commun.*, 2019, **55**, 11119–11122.
20 X. Gong, R. M. Young, K. J. Hartlieb, C. Miller, Y. Wu, H. Xiao, P. Li, N. Hafezi, J. Zhou, L. Ma, T. Cheng, W. A. III Goddard, O. K. Farha, J. T. Hupp, M. R. Wasielewski and J. F. Stoddart, Intramolecular energy and electron transfer within a diazaperopyrenium-based cyclophane, *J. Am. Chem. Soc.*, 2017, **139**, 4107–4116.
21 X. Wang, S. Wang, J. Lv, S. Shao, L. Wang, X. Jing and F. Wang, Through-space charge transfer hexaarylbenzene dendrimers with thermally activated delayed fluorescence and aggregation-induced emission for efficient solution-processed OLEDs, *Chem. Sci.*, 2019, **10**, 2915–2923.
22 Z. Wang, X. Gou, Q. Shi, K. Liu, X. Chang, G. Wang, W. Xu, S. Lin, T. Liu and Y. Fang, Through-space charge transfer: a new way to develop a high-performance fluorescence sensing film towards opto-electronically inert alkanes, *Angew. Chem., Int. Ed.*, 2022, **61**, e202207619.
23 F.-M. Xie, H.-Z. Li, K. Zhang, Y. Shen, X. Zhao, Y.-Q. Li and J.-X. Tang, A dislocated twin-locking acceptor-donor-acceptor configuration for efficient delayed fluorescence with multiple through-space charge transfer, *Angew. Chem., Int. Ed.*, 2022, **61**, e202213823.
24 Y.-J. Yu, M. Song, X.-Y. Meng, Y.-K. Qu, X.-Q. Wang, L. Chen, S.-Y. Yang, D.-Y. Zhou, Z.-Q. Jiang and L.-S. Liao, Design and synthesis of red through-space charge transfer thermally activated delayed fluorescence emitters with donor/acceptor/donor stacking, *Org. Lett.*, 2023, **25**, 6024–6028.
25 L. Cheng, K. Liu, Y. Duan, H. Duan, Y. Li, M. Gao and L. Cao, Adaptive chirality of an achiral cage: chirality transfer, induction, and circularly polarized luminescence through aqueous host–guest complexation, *CCS Chem.*, 2020, **3**, 2749–2763.
26 N. Han, J. Ma, H. Yu, J. Shi, Q. Bai, X. Jiang, Z. Zhang, P. Wang, J. Yu and M. Wang, Sandwich-like heterochromophore metallo-supramolecules based on

dense chromophore arrangements with energy and chirality transfer properties, *CCS Chem.*, 2024, **6**, 1264–1277.

27 G. Ouyang, J. Rühe, Y. Zhang, M.-J. Lin, M. Liu and F. Würthner, Intramolecular energy and solvent-dependent chirality transfer within a BINOL-perylene heterocyclophane, *Angew. Chem., Int. Ed.*, 2022, **61**, e202206706.

28 J. Fan, M. Hu, P. Zhan and X. Peng, Energy transfer cassettes based on organic fluorophores: construction and applications in ratiometric sensing, *Chem. Soc. Rev.*, 2013, **42**, 29–43.

29 C. G. dos Remedios and P. D. J. Moens, Fluorescence resonance energy transfer spectroscopy is a reliable "ruler" for measuring structural changes in proteins: dispelling the problem of the unknown orientation factor, *J. Struct. Biol.*, 1995, **115**, 175–185.

30 W.-J. Guo, S. Yan, L. Chen, L. Qiao, S. Xu, T. Qi, B. Liu and H.-Q. Peng, Isomeric engineering of organic luminophores for multicolor room temperature phosphorescence including red afterglow, *Adv. Funct. Mater.*, 2024, **34**, 2406888.

31 Y. Liu, J. Yang, Z. Mao, Y. Wang, J. Zhao, S.-J. Su and Z. Chi, Isomeric thermally activated delayed fluorescence emitters for highly efficient organic light-emitting diodes, *Chem. Sci.*, 2023, **14**, 1551–1556.

32 H. Yu, P. Tian, N. Han, M. Li and M. Wang, Nitrogen atom induced contrast effect on the mechanofluorochromic characteristics of anthracene-based acceptor-donor-acceptor fluorescent molecules, *Chem.–Asian J.*, 2023, **18**, e202300712.

33 S. K. Pathak, G. Li, C. Zhou, Z. Wang and H. Liu, Regioisomer enabling efficient red TADF emitters based on pyridobenzoquinoxaline, *J. Mater. Chem. C*, 2023, **11**, 6685–6694.

34 H. Zhu, J. Liu, Y. Wu, L. Wang, H. Zhang, Q. Li, H. Wang, H. Xing, J. L. Sessler and F. Huang, Substrate-responsive pillar[5]arene-based organic room-temperature phosphorescence, *J. Am. Chem. Soc.*, 2023, **145**, 11130–11139.

35 S. Adak, I. Ghosh, M. L. Maity and S. Bandyopadhyay, Arylazopyrazole photoconversion enables tunable morphology and mechanical properties, *Small*, 2025, **21**, 2412482.

36 D. R. S. Pooler, D. Doellerer, S. Crespi and B. L. Feringa, Controlling rotary motion of molecular motors based on oxindole, *Org. Chem. Front.*, 2022, **9**, 2084–2092.

37 F. Xu, L. Pfeifer, S. Crespi, F. K.-C. Leung, M. C. A. Stuart, S. J. Wezenberg and B. L. Feringa, From Photoinduced supramolecular polymerization to responsive organogels, *J. Am. Chem. Soc.*, 2021, **143**, 5990–5997.

38 N. A. Simeth, S. Kobayashi, P. Kobauri, S. Crespi, W. Szymanski, K. Nakatani, C. Dohno and B. L. Feringa, Rational design of a photoswitchable DNA glue enabling high regulatory function and supramolecular chirality transfer, *Chem. Sci.*, 2021, **12**, 9207–9220.

39 S. J. Wezenberg, L.-J. Chen, J. E. Bos, B. L. Feringa, E. N. W. Howe, X. Wu, M. A. Siegler and P. A. Gale, Photomodulation of transmembrane transport and potential by stiff-stilbene based bis(thio)ureas, *J. Am. Chem. Soc.*, 2022, **144**, 331–338.

40 T. Bartelmann, F. Gnannt, M. Zitzmann, P. Mayer and H. Dube, Sulfoxide hemithioindigo tweezers – visible light addressable capture and release, *Chem. Sci.*, 2021, **12**, 3651–3659.

41 Y. Li, S. Liu, H. Ni, H. Zhang, H. Zhang, C. Chuah, C. Ma, K. S. Wong, J. W. Y. Lam, R. T. K. Kwok, J. Qian, X. Lu and B. Z. Tang, ACQ-to-AIE transformation: tuning molecular packing by regioisomerization for two-photon NIR bioimaging, *Angew. Chem., Int. Ed.*, 2020, **59**, 12822–12826.

42 P. Howlader, S. Ahmed, S. Mondal, E. Zangrando and P. S. Mukherjee, Conformation-selective self-assembly of Pd_6 trifacial molecular barrels using a tetrapyridyl ligand, *Inorg. Chem.*, 2022, **61**, 8121–8125.

43 H. Lee, J. Tessarolo, D. Langbehn, A. Baksi, R. Herges and G. H. Clever, Light-powered dissipative assembly of diazocine coordination cages, *J. Am. Chem. Soc.*, 2022, **144**, 3099–3105.

44 E. Benchimol, J. Tessarolo and G. H. Clever, Photoswitchable coordination cages, *Nat. Chem.*, 2024, **16**, 13–21.

45 Z.-T. Shi, Y.-X. Hu, Z. Hu, Q. Zhang, S.-Y. Chen, M. Chen, J.-J. Yu, G.-Q. Yin, H. Sun, L. Xu, X. Li, B. L. Feringa, H.-B. Yang, H. Tian and D.-H. Qu, Visible-light-driven rotation of molecular motors in discrete supramolecular metallacycles, *J. Am. Chem. Soc.*, 2021, **143**, 442–452.

46 R. G. DiNardi, A. O. Douglas, R. Tian, J. R. Price, M. Tajik, W. A. Donald and J. E. Beves, Visible-light-responsive self-assembled complexes: improved photoswitching properties by metal ion coordination, *Angew. Chem., Int. Ed.*, 2022, **61**, e20220501.

47 D. Mutruc, A. Goulet-Hanssens, S. Fairman, S. Wahl, A. Zimathie, C. Knie and S. Hecht, Modulating guest uptake in core–shell MOFs with visible light, *Angew. Chem., Int. Ed.*, 2019, **58**, 12862–1867.

48 Y. Jiang, W. Danowski, B. L. Feringa and L. Heinke, Nanoporous films with oriented arrays of molecular motors for photoswitching the guest adsorption and diffusion, *Angew. Chem., Int. Ed.*, 2023, **62**, e202214202.

49 H. D. Cornell, A. T. Sose, S. Ilic, S. Chinnabattigalla, N. E. Lidman, C. M. Oldmixon, X. Yang, S. A. Deshmukh and A. J. Morris, Photoactivated multivariate metal–organic frameworks for on-demand drug release: the role of host–guest interactions, *J. Am. Chem. Soc.*, 2025, **147**, 7423–7432.

50 W. Danowski, F. Castiglioni, A. S. Sardjan, S. Krause, L. Pfeifer, D. Roke, A. Comotti, W. R. Browne and B. L. Feringa, Visible-light-driven rotation of molecular motors in a dual-function metal–organic framework enabled by energy transfer, *J. Am. Chem. Soc.*, 2020, **142**, 9048–9056.

51 I. Jahović, Y. Yang, T. K. Ronson and J. R. Nitschke, Capture of singlet oxygen modulates host-guest behavior of coordination cages, *Angew. Chem., Int. Ed.*, 2023, **62**, e202309589.

52 M. Kimura, M. Sano, T. Muto, K. Hanabusa and H. Shirai, Self-Assembly of Twisted Bridging Ligands to Helical

Coordination Polymers, *Macromolecules*, 1999, **32**, 7951–7953.

53 J. Ma, N. Han, H. Yu, J. Li, J. Shi, S. Wang, H. Zhang and M. Wang, Multi-decker emissive supramolecular architectures based on shape-complementary ligands pair, *Small*, 2022, **18**, 2202167.

54 S. Pullen, J. Tessarolo and G. H. Clever, Increasing structural and functional complexity in self-assembled coordination cages, *Chem. Sci.*, 2021, **12**, 7269–7293.

55 X. Tian, K. Shoyama, B. Mahlmeister, F. Brust, M. Stolte and F. Würthner, Naphthalimide-annulated [n]helicenes: red circularly polarized light emitters, *J. Am. Chem. Soc.*, 2023, **145**, 9886–9894.

56 L. Chen, C. Li, Z.-F. Liu, Y. Kuboi, E. Fu, L. S. Vargas, C. Adachi, F. Mathevet and S. Zhang, A donor–acceptor cage for circularly polarized TADF emission, *Chem. Commun.*, 2024, **60**, 1758–1761.

57 I. A. Bhat, A. Devaraj, P. Howlader, K.-W. Chi and P. S. Mukherjee, Preparation of a chiral Pt_{12} tetrahedral cage and its use in catalytic Michael addition reaction, *Chem. Commun.*, 2018, **54**, 4814–4817.

58 P. Howlader, E. Zangrando and P. S. Mukherjee, Self-assembly of enantiopure Pd_{12} tetrahedral homochiral nanocages with tetrazole linkers and chiral recognition, *J. Am. Chem. Soc.*, 2020, **142**, 9070–9078.

59 P. Howlader, S. Mondal, S. Ahmed and P. S. Mukherjee, Guest-Induced Enantioselective Self-Assembly of a Pd_6 Homochiral octahedral cage with a C_3-symmetric pyridyl donor, *J. Am. Chem. Soc.*, 2020, **142**, 20968–20972.

60 H. Duan, Y. Li, Q. Li, P. Wang, X. Liu, L. Cheng, Y. Yu and L. Cao, Host–guest recognition and fluorescence of a tetraphenylethene-based octacationic cage, *Angew. Chem., Int. Ed.*, 2020, **59**, 10101–10110.

61 L. Cheng, P. Tian, H. Duan, Q. Li, X. Song, A. Li and L. Cao, Chiral adaptive recognition with sequence specificity of aromatic dipeptides in aqueous solution by an achiral cage, *Chem. Sci.*, 2023, **14**, 833–842.

62 Z. Li, Y. Yan, Z. Chen, R. Tang, N. Han, R. Han, F. Fang, J. Jiang, L. Hua, X. Yu, M. Wang, J. Cai, H. Li, H. Wang and X. Li, Multidimensional decryption of metallopolymer at single-chain level, *CCS Chem.*, 2025, **7**, 2381–2393.

63 M. Weh, K. Shoyama and F. Würthner, Preferential molecular recognition of heterochiral guests within a cyclophane receptor, *Nat. Commun.*, 2023, **14**, 243.

64 M. Weh, A. A. Kroeger, K. Shoyama, M. Grüne, A. Karton and F. Würthner, π-π catalysis made asymmetric—enantiomerization catalysis mediated by the chiral π-system of a perylene bisimide cyclophane, *Angew. Chem., Int. Ed.*, 2023, **62**, e202301301.

65 M. Sapotta, P. Spenst, C. R. Saha-Möller and F. Würthner, Guest-mediated chirality transfer in the host–guest complexes of an atropisomeric perylene bisimide cyclophane host, *Org. Chem. Front.*, 2019, **6**, 892–899.

66 CCDC 2440691, Experimental Crystal Structure Determination, 2025, DOI: **10.5517/ccdc.csd.cc2mxqz8**.